Electronic version of paper:
Z. Chen H. Waubke W. Kreuzer: **A Formulation of the Fast Multipole Boundary Element Method (FMBEM) for Acoustic Radiation and Scattering from Three-dimensional Structures** in Journal of Computational Acoustic 16(2), 2008
doi: 10.1142/S0218396X08003725

Journal of Computational Acoustics

A FORMULATION OF THE FAST MULTIPOLE BOUNDARY ELEMENT METHOD (FMBEM) FOR ACOUSTIC RADIATION AND SCATTERING FROM THREE-DIMENSIONAL STRUCTURES

Z.-S. CHEN

Acoustics Research Institute, Austrian Academy of Sciences,
Reichsratsstrasse 17, A-1010 Vienna, Austria
zhensheng.chen@oeaw.ac.at
http://www.kfs.oeaw.ac.at

H. WAUBKE

Acoustics Research Institute, Austrian Academy of Sciences,
Reichsratsstrasse 17, A-1010 Vienna, Austria
Email: holger.waubke@oeaw.ac.at

W. KREUZER

Acoustics Research Institute, Austrian Academy of Sciences,
Reichsratsstrasse 17, A-1010 Vienna, Austria
Email: wolfgang.kreuzer@oeaw.ac.at

Received 30. June 2005
Revised (10. November 2006)

Compared to the traditional boundary element method (BEM), the single level fast multipole boundary element method (SLFMBEM) or the multilevel fast multipole boundary element method (MLFMBEM) reduces the computational complexity of a job from $O(n^2)$ to $O(n^{3/2})$ or $O(n \log^2 n)$ respectively with n being the number of unknowns; this means a dramatical reduction in terms of CPU-time and storage requirement. Large scale problems, unsolvable with the traditional BEM, can be solved by using the FMBEM. In this paper the traditional BEM, SLFMBEM and MLFMBEM are formulated within the framework of the Burton-Miller Collocation BEM for acoustic radiation and scattering from 3-dimensional structures. Attention is especially paid to the practical aspects of the method in order to get a reliable and efficient computation code. The performance of the method is tested with practical examples, including one for computing the head-related transfer function (HRTF) between 1000 Hz and 18000 Hz.

Keywords: Fast multipole algorithm; boundary element method; Helmholtz equation.

1. Introduction

The boundary element method (BEM) is a very popular numerical tool in computational acoustics. The traditional BEM can unfortunately only be used for problems in the low frequency region because the CPU-time and storage requirement increases approximately proportional to n^2 (if iterative solvers are used). Here n denotes the number of unknowns of a model, which is again proportional to the square of the frequency for 3D problems.

The fast multipole method, which was originally developed by Rokhlin to accelerate the computation of potential fields[1], is applied successfully to overcome the above difficulty of the traditional BEM for acoustics and electromagnetics[2−18].

Giebermann[7] has given a detailed description of the SLFMBEM for the Helmholtz equation. He indicated that the SLFMBEM achieves its optimal numerical complexity of $O(n^{3/2})$ when the number of element clusters is approximately equal to $\sqrt{n}$. Detailed descriptions of the MLFMBEM including the error analysis and complexity estimation are given among others by Epton and Dembart[5], Rahola[6], Darve[13], Koc and Chew[11], Sakuma and Yasuda[14] [15] (the complexity estimation of $O(n \log^2 n)$ can be found in[13]). Schneider[16] applied the MLFMBEM to the collocation BEM whereas Fischer *et al.*[17] [19] employed the method on the Galerkin BEM; both papers are aimed at adapting the theoretical results to engineering applications.

The goal of the present work is of a practical nature, *i. e.* to develop a reliable and efficient computer code by using the theoretical results for the SLFMBEM and MLFMBEM. The Burton-Miller approach[20] is used to suppress the singularities of the coefficient matrix at the irregular frequencies. Using this approach the users are free from the difficult task of selecting appropriate CHIEF-points[21]. The discontinuous elements with the collocation points in the interior of the element are used to model the surfaces of the volumes or/and the middle faces of the thin-walled structures. Thus the evaluation of the hyper singular integrals becomes a solvable task and the burdensome multivalue problem at nodes located on the intersections is avoided. Moreover, according to[22], a mesh consisting of discontinuous elements gives even more accurate results than a corresponding mesh consisting of continuous elements with roughly the same total number of unknowns.

The present paper has the following features:

- The (traditional) BEM, SLFMBEM and MLFMBEM are formulated for radiation and scattering problems from structures consisting of 3D volumes or/and thin walled parts with/without admittance boundary conditions, namely for a rather general case of practical applications, whereas in the literature up to now the fast method is applied almost exclusively to 3D volumes.
- In the (traditional) BEM it is well known that the symmetry or/and antisymmetry planes orthogonal to the three coordinates can be used to reduce the model scale, *i. e.* a model can be reduced to a half, quarter or eighth of the original one when there are one, two or three symmetric or/and antisymmetric planes. In our computer code such possibility for BEM is adopted to FMBEM. Results of an example with two symmetric planes simulated by using a quarter model were published in a earlier paper about SLFMBEM[23]. Recently Yasuda described the algorithm in detail in a paper about MLFMBEM applied to sound field with one symmetric plane[24]. In this paper the 'reflections' of the boundary elements and element clusters with respect to the symmetry/antisymmetry planes are shortly described. Results of an example with 2 symmetry planes are shown in the last part of this paper.
- In our computer code the results of the FEM structural analysis can be directly used as

boundary conditions for the BEM acoustic analysis, this is presented in[23].

- The interpolation/filtering computations between the father and son levels determines the efficiency and stability of the MLFMBEM algorithm. The interpolation procedure using the spherical harmonic functions is stable but numerically intensive. A so called direct MLFMBEM scheme, by which the coefficient matrices at each level are stored and the interpolation/filtering procedures between the son/father levels are avoided, is proposed to accelerate the MLFMBEM. The two examples cited in this paper indicate that this scheme can really accelerates the computations substantially at the cost of a moderate increase of the storage requirements.

The following four sections are devoted to

- formulation of the Burton-Miller collocation BEM;
- formulation of the SLFMBEM within the framework of the Burton-Miller collocation BEM;
- formulation of the MLFMBEM;
- two numerical examples.

2. A formulation of the three-dimensional Burton-Miller collocation BEM

The basic equation for acoustic problems in the frequency domain is the Helmholtz equation

$$\nabla^2\phi(\mathbf{y}) + k^2\phi(\mathbf{y}) = 0\,, \tag{1}$$

where $\phi(\mathbf{y})$ denotes the velocity potential at the point $\mathbf{y}$ and $k = \omega/c$ is the wave number depending on sound speed c and angular frequency ω. Between the sound pressure p and the velocity potential exists the relation $p = i\omega\rho\phi$ with ρ denoting the density of the medium and $i^2 = -1$ (the harmonic time dependence $e^{-i\omega t}$ is implied). The following integral equations for the Helmholtz equation were derived by Chen *et al.* (eqs. (20), (21) and (22) [25]):

$$-\frac{1}{2}\phi(\mathbf{x}) + L[\phi,\tilde{\phi},\bar{\phi}](\mathbf{x}) = -\phi_i(\mathbf{x}) + \tau L[v_0](\mathbf{x}), \quad \mathbf{x}\in S_1, \tag{2}$$

$$-\frac{1}{2}\bar{\phi}(\mathbf{x}) + L[\phi,\tilde{\phi},\bar{\phi}](\mathbf{x}) = -\phi_i(\mathbf{x}) + \tau L[v_0](\mathbf{x}), \quad \mathbf{x}\in S_2, \tag{3}$$

$$\frac{1}{2}\hat{\phi}(\mathbf{x}) + \frac{\partial}{\partial n_x}L[\phi,\tilde{\phi},\bar{\phi}](\mathbf{x}) = -v_i(\mathbf{x}) + v_0(\mathbf{x}) + \tau\frac{\partial}{\partial n_x}L[v_0](\mathbf{x}), \quad \mathbf{x}\in S_2\,. \tag{4}$$

with $\hat{\phi}(\mathbf{x}) := \tilde{A}(\mathbf{x})\bar{\phi}(\mathbf{x}) + \bar{A}(\mathbf{x})\tilde{\phi}(\mathbf{x})$. In the above equations S_1 represents the surfaces of the 3-dimensional volumes and S_2 the middle faces of the thin walled parts. $\mathbf{x}$ denotes an arbitrary point of S_1 or S_2 with a unique normal to S_1 or S_2, n_x. It is assumed that n_x at S_1 always point to the exterior domain whereas the side of S_2 into which n_x points is defined as the positive side. The coefficient τ is used to adjust the domain to which the formulation is applied ($\tau = 1$ for the exterior problems and $\tau = -1$ for the interior problems). ϕ, $\tilde{\phi}$ and $\bar{\phi}$ stand for the velocity potential at S_1, the difference and the sum of velocity potentials on the positive and the negative sides of S_2 respectively ($\tilde{\phi} := \phi^+ - \phi^-$

and $\bar{\phi} := \phi^+ + \phi^-$ with ϕ^+ and ϕ^- being the velocity potentials on the positive and the negative sides of S_2). ϕ_i and $v_i = \partial\phi_i/\partial n_x$ are the velocity potential and the particle velocity in the direction n_x of the incident sound waves whereas $v_0(\mathbf{x})$ denotes the velocity of the surface or middle face of the structure at the point $\mathbf{x}$ in the direction n_x. $A(\mathbf{x}) = i\omega\rho a(\mathbf{x}) = v(\mathbf{x})/\phi(\mathbf{x})$ with $a(\mathbf{x}) = v(\mathbf{x})/p(\mathbf{x})$ is the via ϕ defined admittance at the point $\mathbf{x}$, while $\tilde{A}(\mathbf{x}) := [A^+(\mathbf{x}) - A^-(\mathbf{x})]/2$ and $\bar{A}(\mathbf{x}) := [A^+(\mathbf{x}) + A^-(\mathbf{x})]/2$ stand for half of the difference and the average of admittances on the positive and the negative sides of the middle face S_2. The integral operator $L[\phi, \tilde{\phi}, \bar{\phi}](\mathbf{x})$ is defined as

$$L[\phi, \tilde{\phi}, \bar{\phi}](\mathbf{x}) := L[\phi](\mathbf{x}) + L[\tilde{\phi}](\mathbf{x}) + L[\bar{\phi}](\mathbf{x}) \tag{5}$$

with

$$L[\phi](\mathbf{x}) := \int_{S_1} [G(\mathbf{y}, \mathbf{x})A(\mathbf{y}) + \tau H(\mathbf{y}, \mathbf{x})]\phi(\mathbf{y})dS_y, \tag{6}$$

$$L[\tilde{\phi}](\mathbf{x}) := \int_{S_2} [G(\mathbf{y}, \mathbf{x})\tilde{A}(\mathbf{y}) + H(\mathbf{y}, \mathbf{x})]\tilde{\phi}(\mathbf{y})dS_y, \tag{7}$$

$$L[\bar{\phi}](\mathbf{x}) := \int_{S_2} G(\mathbf{y}, \mathbf{x})\bar{A}(\mathbf{y})\bar{\phi}(\mathbf{y})dS_y. \tag{8}$$

The integral operator $L[v_0](\mathbf{x})$ is defined as

$$L[v_0](\mathbf{x}) := \int_{S_1} G(\mathbf{y}, \mathbf{x})v_0(\mathbf{y})dS_y. \tag{9}$$

In these equations the functions $G(\mathbf{y}, \mathbf{x})$ and $H(\mathbf{y}, \mathbf{x})$ are the Green function of the Helmholtz equation and its derivatives with respect to n_y:

$$G(\mathbf{y}, \mathbf{x}) = \frac{e^{ikr}}{4\pi r}, \tag{10}$$

$$H(\mathbf{y}, \mathbf{x}) = \frac{\partial G(\mathbf{y}, \mathbf{x})}{\partial n_y} = \frac{e^{ikr}}{4\pi r}\left(ik - \frac{1}{r}\right)\frac{\partial r}{\partial n_y} \tag{11}$$

with $r = \|\mathbf{y} - \mathbf{x}\|$ the distance between the source point $\mathbf{y}$ and the field point $\mathbf{x}$. If S_2 is acoustically hard ($\tilde{A}(\mathbf{y})$ and $\bar{A}(\mathbf{y})$ are zero), then the integral in (8) is zero and $\bar{\phi}(\mathbf{y})$ does not appear in the integral equations. In this case $\tilde{\phi}(\mathbf{y})$ is the only unknown function on S_2.

In order to apply the Burton-Miller method, eq. (2) is differentiated with respect to n_x, yielding

$$-\frac{1}{2}[v_0(\mathbf{x}) - \tau A(\mathbf{x})\phi(\mathbf{x})] + \frac{\partial}{\partial n_x}L[\phi, \tilde{\phi}, \bar{\phi}](\mathbf{x}) = -v_i(\mathbf{x}) + \tau\frac{\partial}{\partial n_x}L[v_0](\mathbf{x}), \quad \mathbf{x} \in S_1 \tag{12}$$

where the relations $\partial\phi(\mathbf{x})/\partial n_x = v(\mathbf{x}) = v_0(\mathbf{x}) - \tau A(\mathbf{x})\phi(\mathbf{x})$ and $\partial\phi_i(\mathbf{x})/\partial n_x = v_i(\mathbf{x})$ are applied. Setting the coupling factor to $\beta = i/k$, multiplying (12) with $\tau\beta$ and adding the result to (2) gives a combined equation

$$\frac{1}{2}[\beta A(\mathbf{x}) - 1]\phi(\mathbf{x}) + L[\phi, \tilde{\phi}, \bar{\phi}](\mathbf{x}) + \tau\beta\frac{\partial}{\partial n_x}L[\phi, \tilde{\phi}, \bar{\phi}](\mathbf{x}) = \tau\beta[\frac{1}{2}v_0(\mathbf{x}) - v_i(\mathbf{x})] -$$

$$\phi_i(\mathbf{x}) + \tau L[v_0](\mathbf{x}) + \beta \frac{\partial}{\partial n_x} L[v_0](\mathbf{x}). \quad \mathbf{x} \in S_1 \tag{13}$$

The equations (13), (4) and (3) are the basic integral equations for the collocation BEM discretization of the Helmholtz equation. If the collocation point is located at S_1, eq. (13) is applied to the unknown $\phi(\mathbf{x})$; if it lies at S_2, eqs. (4) and (3) are applied to the two unknowns $\tilde{\phi}(\mathbf{x})$ and $\bar{\phi}(\mathbf{x})$ respectively. If both surfaces of S_2 at the collocation point are acoustically hard, only eq. (4) is relevant because in this case $\tilde{\phi}(\mathbf{x})$ is the only unknown. Whereas all other integrals appearing in (13), (4) and (3) can be directly evaluated by using the Gauss-Legendre integrations, the hyper singular integral $N(\mathbf{x}) = (\partial/\partial n_x)[\int_{S_e} \partial G(\mathbf{y}, \mathbf{x})/\partial n_y \, \phi(\mathbf{y}) \, dS_y]$ (S_e represents the surface of an element) must first be converted into the sum of a weakly singular surface integral and a line integral. For constant elements the following equation can be derived by using the Stokes formula[26]:

$$N(\mathbf{x}) = \phi(\mathbf{x})[n_{xi}\varepsilon_{ijk} \oint_{\partial S_e} \frac{\partial G(\mathbf{y}, \mathbf{x})}{\partial y_j} dy_k + k^2 \int_{S_e} G(\mathbf{y}, \mathbf{x}) \mathbf{n}_x \mathbf{n}_y dS_y], \tag{14}$$

where ε_{ijk} stands for the iteration symbol.

3. Single Level Fast Multilpole BEM (SLFMBEM)

The FMBEM uses the fact that the kernel functions in the integral equations (13), (4) and (3) in $\mathbb{R}^3 \backslash B_{\rho_1}(\mathbf{z}_1)$ (see Fig. 1) can be expressed by their far field patterns around the center $\mathbf{z}_1$ near to the source points $\mathbf{y}_i$; these far field patterns can then be converted to the corresponding near field patterns in $B_{\rho_2}(\mathbf{z}_2)$ around the center $\mathbf{z}_2$ near to the field points $\mathbf{x}_j$, if $\delta := ||\mathbf{z}_2 - \mathbf{z}_1|| > \rho_1 + \rho_2$. The values of the kernel functions with the source points in $B_{\rho_1}(\mathbf{z}_1)$ and the field points in $B_{\rho_2}(\mathbf{z}_2)$ can then be evaluated by using these near field patterns.

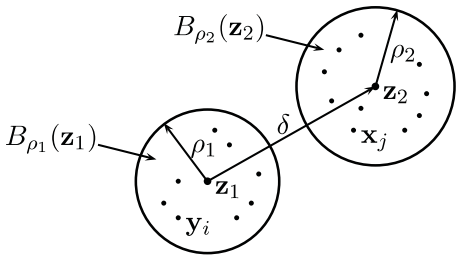

Fig. 1. Spheres around the source and field points.

If F represents an arbitrary solution of the Helmholtz equation in $\mathbb{R}^3 \backslash B_{\rho_1}(\mathbf{z}_1)$, then its far field pattern can be defined as[7]

$$\Psi[F](\hat{\mathbf{z}}) := \lim_{t \to \infty} \frac{F(\mathbf{z}_1 + t\hat{\mathbf{z}})}{h_0(t)}, \tag{15}$$

where $h_0(t) = e^{ikt}/(ikt)$ is the spherical Hankel function of the first kind and order 0. The unit vector $\hat{\mathbf{z}}$ represents an arbitrary direction; it can also be realized as an arbitrary point on the unit sphere surface $\mathbb{S}$. For the far field pattern Ψ (and also for the later introduced near field pattern) there is a translation relation

$$\Psi_m[F](\hat{\mathbf{z}}) = \Psi_l[F](\hat{\mathbf{z}}) e^{ik(\mathbf{z}_m - \mathbf{z}_l)\hat{\mathbf{z}}}\,, \tag{16}$$

where $\mathbf{z}_l$ and $\mathbf{z}_m$ are two reference centers and $\Psi_l[F](\hat{\mathbf{z}})$ and $\Psi_m[F](\hat{\mathbf{z}})$ the far field patterns around $\mathbf{z}_l$ and $\mathbf{z}_m$ respectively. According to the above definition of the far field pattern and the translation relation, the far field patterns of $G(\mathbf{y}, \mathbf{x})$ and $H(\mathbf{y}, \mathbf{x})$ can be expressed as

$$\begin{aligned} \Psi[G](\hat{\mathbf{z}}) &= \frac{ik}{4\pi} e^{ik(\mathbf{z}_1 - \mathbf{y})\hat{\mathbf{z}}}\,, \\ \Psi[H](\hat{\mathbf{z}}) &= \frac{k^2 \hat{\mathbf{z}} \mathbf{n}_y}{4\pi} e^{ik(\mathbf{z}_1 - \mathbf{y})\hat{\mathbf{z}}}\,. \end{aligned} \tag{17}$$

Under the condition that $\delta > \rho_1 + \rho_2$, the truncated representation of the near field pattern of F in $B_{\rho_2}(\mathbf{z}_2)$ can be defined as

$$\Upsilon_N[F](\hat{\mathbf{z}}) := \sum_{j=0}^{N-1} i^j (2j+1) h_j(k\|\mathbf{z}_2 - \mathbf{z}_1\|) P_j[\widehat{(\mathbf{z}_2 - \mathbf{z}_1)}\hat{\mathbf{z}}] \Psi[F](\hat{\mathbf{z}})\,, \tag{18}$$

where h_j stands for the spherical Hankel function of the first kind and order j and P_j for the Legendre polynomial of order j. The following recurrence relations could be used to compute them[28], if the computations could be shown to be stable:

$$h_j(x) = (2j-1) h_{j-1}(x)/x - h_{j-2}(x) \tag{19}$$

with $h_0(x) = [\sin(x)/x] + i\,[-\cos(x)/x]$ and $h_1(x) = [\sin(x)/x^2 - \cos(x)/x] + i\,[-\cos(x)/x^2 - \sin(x)/x]$ for the spherical Hankel functions and

$$p_j(x) = [(2j-1) x p_{j-1}(x) - (j-1) p_{j-2}(x)]/j \tag{20}$$

with $p_0(x) = 1$ and $p_1(x) = x$ for the the Legendre polynomials. Our numerical tests indicate, that the computations (19) and (20) are stable for the imaginary part of $h_j(x)$ and for the Legendre polynomials $p_j(x)$. However, for computation of the real part of $h_j(x)$, the equation (19) is shown to be very unstable. The method described in [7], pp. 87-88, can be used to overcome this difficulty.

It can be proven that in $B_{\rho_2}(\mathbf{z}_2)$ the Function $F(\mathbf{x})$ can be approximated by the integral over the unit sphere surface $\mathbb{S}$ [7]

$$F_N(\mathbf{x}) := \frac{1}{4\pi} \int_{\mathbb{S}} \Upsilon_N[F](\hat{\mathbf{z}}) e^{ik(\mathbf{x} - \mathbf{z}_2)\hat{\mathbf{z}}}\, d\hat{\mathbf{z}}\,, \tag{21}$$

i. e.

$$\begin{aligned} \lim_{N\to\infty} |F(\mathbf{x}) - F_N(\mathbf{x})| &= 0\,, \\ \lim_{N\to\infty} |\nabla F(\mathbf{x}) - \nabla F_N(\mathbf{x})| &= 0 \end{aligned} \tag{22}$$

with $\nabla F_N(\mathbf{x}) = ik/(4\pi) \int_{\mathbb{S}} \Upsilon_N[F](\hat{\mathbf{z}}) e^{ik(\mathbf{x}-\mathbf{z}_2)\hat{\mathbf{z}}} \hat{\mathbf{z}}\, d\hat{\mathbf{z}}$.

In order to realize the SLFMBEM algorithm, the BE mesh must be divided into element clusters. The number of clusters should be approximately equal to the root of the number of elements because the efficiency of the algorithm arrives with this number at its maximum [7]. In order to clustering an element group (with our program the user can define element groups arbitrarily), a cuboid (with faces parallel to the coordinate planes) containing all elements of the group, is subdivided into subcuboids, whose edge length approximately equals to $\sqrt[4]{n}\, l$ with n denoting the number of boundary elements and l the average dimension of the boundary elements. Elements, whose center points are located is the same subcuboid, form a cluster. Clusters with very few elements can be incorporated into clusters that are located near to them. The number of clusters, which are generated by using the above algorithm, is approximately equal to $\sqrt{n}$. For any cluster, say the cluster C_i, a far field and a near field can be defined as follows: any cluster C_j satisfying the condition $\|\mathbf{z}_j - \mathbf{z}_i\| > c(\rho_j + \rho_i)$ belongs to the far field, otherwise to the near field. Here $\mathbf{z}_{i(j)}$ and $\rho_{i(j)}$ denote the center and the radius of the cluster $i(j)$ respectively, $c > 1$ is a parameter to be chosen ($c = \sqrt{5}/2.0$ is used in the present work). For the clusters in the near field of a given cluster the traditional BEM is used, whereby a sparse near field coefficient matrix and the corresponding part of the right hand side vector are generated. To the clusters in the far field the FMBEM algorithm is applied, by which the far field matrices and the corresponding part of the right hand side vector are computed.

The problem of choosing an appropriate value for N in (18) is addressed by many authors[4 8 12 15]. In the present work it is estimated by using the empirical equation

$$N = max(2k\rho_{max} + 1.8 * log(2k\rho_{max} + \pi),\ N_0). \tag{23}$$

with ρ_{max} the maximum radius of the clusters. Our numerical experiments indicate that the equation $N = 2k\rho_{max} + 1.8 * log(2k\rho_{max} + \pi)$ gives a good estimation of N except for very low frequencies. This problem can be solved by setting N to a given value N_0 (with $N_0 = 7$ or 8 for example) when it yields a value less than N_0. The integral over the unit sphere surface $\mathbb{S}$ in (21) can be evaluated numerically: in the ϑ-direction by using a Gauss-Legendre integration with N points and in the φ-direction by using a trapeze integration rule with $2N$ equal intervals:

$$\int_{\mathbb{S}} f(\hat{\mathbf{z}}) d\hat{\mathbf{z}} = \int_{-1}^{1} \int_{0}^{2\pi} f(\hat{\mathbf{z}}) d\varphi d(\cos(\vartheta)) \approx \pi/N \sum_{i=1}^{N} \sum_{j=1}^{2N} w_i\, f(\hat{\mathbf{z}}_{i,j}) \tag{24}$$

with w_i the weight of the Gauss-Legendre integration for the i-th integration point in the ϑ-direction.

Now we will see how the SLFMBEM is applied to the far field of a cluster, say the cluster i. It consists of three steps. In the first step, equation (17) is applied to the kernel functions appearing in equations (13), (4) and (3) to compute the far field patterns of the integrals $L[\phi](\mathbf{x})$, $L[\tilde{\phi}](\mathbf{x})$, $L[\bar{\phi}](\mathbf{x})$ and $L[v_0](\mathbf{x})$ for each cluster. In the second step, equation (18) is applied to all clusters located in the far field of the cluster i, in order to obtain the

contributions of these clusters to the near field pattern of the cluster i. Finally, in the third step, equation (21) and its derivative with respect to n_x are employed in equations (13), (4) and (3) in order to compute the approximations of all integrals appearing in it, *i. e.* $L[\phi, \tilde{\phi}, \bar{\phi}](\mathbf{x})$ and $L[v_0](\mathbf{x})$, and their derivative with respect to n_x. After application of the above algorithm to all clusters, the final equation system can be expressed as

$$(\mathbf{N} + \mathbf{S}\,\mathbf{D}\,\mathbf{T})\,\hat{\mathbf{x}} = \hat{\mathbf{f}}_n + \hat{\mathbf{f}}_f = \hat{\mathbf{f}}\,, \tag{25}$$

where $\hat{\mathbf{x}}$ is the unknown vector, $\hat{\mathbf{f}}_n$ and $\hat{\mathbf{f}}_f$ are the right hand side vectors generated by using the traditional BEM applied to the near fields and the FMBEM employed to the far fields respectively. The matrix $\mathbf{N}$ represents the near field matrix and the matrices $\mathbf{T}$, $\mathbf{D}$ and $\mathbf{S}$ are generated from the above mentioned first, second and third steps of the SLFMBEM (they are all sparse matrices). If M and m denote the number of clusters and that of integral points on the unit sphere surface $\mathbb{S}$, then $\mathbf{T}$ is a $Mm \times n$ matrix with n being the number of unknowns. $\mathbf{D}$ consists of $M \times M$ submatrices $\mathbf{D}_{i,j}$ (i, $j = 1$, ..., M). Each submatrix $\mathbf{D}_{i,j}$ is a $m \times m$ diagonal matrix, but when the j-th cluster is located in the near field of the i-th cluster then $\mathbf{D}_{i,j} = \mathbf{0}$. Finally $\mathbf{S}$ is a $n \times Mm$ matrix and the far field coefficient matrix $\mathbf{F} = \mathbf{S}\,\mathbf{D}\,\mathbf{T}$ is a $n \times n$ sparse matrix, that need not be explicitly computed.

When a job has 1, 2 or 3 symmetry/antisymmetry planes, it can be discretized with a half, quarter or eighth model (reduced model). In this case, in order to compute the equation system, we take the source elements and clusters as well as the field elements and clusters naturally only from the the reduced model. The field elements and clusters must be 'reflected' with respect to the symmetry/antisymmetry planes in order to obtain there images, whereas the source elements and clusters need not to be reflected. The contributions of the images of the field elements and clusters to the equation system are computed as if they were real elements and clusters. Thus, using a reduced model, the total number of operations for generating the equation system is approximately reduced to a half, quarter or eighth of that of the full model. Denoting the number of unknowns and that of the clusters of a reduced model by $\bar{n}$ and $\bar{M}$ respectively, so the dimension of the matrices $\mathbf{N}$, $\mathbf{T}$, $\mathbf{D}$, and $\mathbf{S}$ are now $\bar{n} \times \bar{n}$, $Mm \times \bar{n}$, $\bar{M}m \times Mm$ and $\bar{n} \times \bar{M}m$ respectively. Compared to the method of [24], which is also based on the reflections of the elements and clusters, our approach is more simple. In the program it can be easily realized by means of a subroutine for reflecting the elements and clusters.

For solving the equation system (25) we have use iterative methods of the Krylov subspace type: the CGS method (Conjugate Gradient Squared), the BiCGSTAB method (Bi-Conjugate Gradient Stabilized) and the QMRCGSTAB method (Quasi-Minimal Residual variant of the BiCGSTAB)[27]. As preconditioning we have applied the incomplete LU-decomposition and the row scanning methods[27], where only the matrix $\mathbf{N}$ is utilized for obtaining the incomplete LU-matrix and the scanning factors for each row. Numerical experiments have indicated that these three iterative methods are efficient and stable; the simple CGS-method is somewhat faster than the other two methods for most examples computed. Although the GMRES method was identified as the best converging iterative solver[29 30], it is not used in the present work because of its larger storage requirement.

The incomplete LU-decomposition preconditioning can considerably reduce the number of iterations and the CPU-time required for achieving a given tolerance ϵ ($\epsilon = 10^{-5}$ is used in the present work).

4. Multilevel Fast Multilpole BEM (MLFMBEM)

For very large jobs the SLFMBEM becomes less efficient because the number of elements in the near field of each cluster increases proportional to $\sqrt{n}$. The MLFMBEM overcomes this difficulty by introducing a cluster tree with several levels. On the finest level the number of elements in the near field of each cluster can be kept very small (independent of the total number of unknowns). Fig. 2 represents a cluster tree with three levels (on each level the father-son relationship is demonstrated by using only one cluster as an example). In order to generate the cluster tree, the clusters on the coarsest level (level 1) are computed from the boundary element mesh by using the same method as for SLFMBEM described in the above section. However the edge length of the subcuboids should be approximately equal to $\sqrt{n/m_1}\, l$ with n being the number of boundary elements and l the average dimension of the elements, in order to obtain approximately m_1 clusters on this level. Then the clusters on each of the other levels are obtained by subdividing their father clusters into two equal parts in each coordinate direction, so 2 to 8 son clusters are generated by every such subdividing. The number of clusters on level 1 should be kept between 20 and several dozen (a larger or smaller number is not recommendable because of worse computational efficiency). For the same reason, each cluster on the finest level should also includes about 20 to several dozen elements.

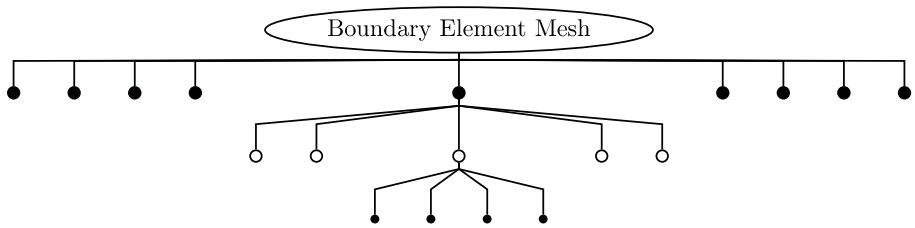

Fig. 2. A cluster tree with 3 levels

The equation system of the MLFMBEM can be expressed similarly to that of the SLFMBEM:

$$[\mathbf{N}_l + \sum_{j=1}^{l} (\mathbf{S}_j \, \mathbf{D}_j \, \mathbf{T}_j)] \, \hat{\mathbf{x}} = \hat{\mathbf{f}} \,, \tag{26}$$

where l is the number of levels. Most concepts introduced in the former section for the SLFMBEM can be now applied to each cluster level. The near field matrix is computed naturally only for the finest level (i. e. the level l), it contains therefore less nonzero components than the corresponding matrix of the SLFMBEM and can be computed more quickly.

The matrices $\mathbf{D}_j$ $(j = 1, 2, ...l)$ represent the transformation matrices form the far field patterns to the near field patterns between clusters that lie in each others interaction field for the levels from 1 to l. The interaction field of a given cluster on a given level is defined as the clusters on the same level which lie in the far field of the considered cluster but their fathers are located in the near field. So only those sub matrices of the matrix $\mathbf{D}_i$ are not zero-matrix, when they correspond to two clusters that lie in the interaction field. As the total number of nonzero components of the matrices $\mathbf{D}_j$ $(j = 1, 2, ...l)$ is not essentially bigger than that of the matrix $\mathbf{D}$ of the SLFMBEM equation system, they are all explicitly computed and stored in our MLFMBEM algorithm. The matrices $\mathbf{T}_j$ and $\mathbf{S}_j$ for $j = 1, 2, ...l$, that correspond to the matrices $\mathbf{T}$ and $\mathbf{S}$ of the SLFMBEM in each cluster level, can be very big for the coarser cluster levels. Therefore they are computed and stored only on the finest level (on this level they are smaller than the corresponding matrices of the SLFMBEM). Accordingly the matrix-vector multiplications in (26) can be carried out explicitly only on the finest level, for the higher levels the corresponding results must be obtained by using a interpolation/filter procedure instead of the direct multiplications.

The interpolation/filter procedure consists of the following steps:

(1) computing $\hat{\mathbf{y}}_{t,l} = \mathbf{T}_l\, \hat{\mathbf{x}}$;
(2) computing $\hat{\mathbf{y}}_{t,j}$ for the levels $j = l-1, ..., 1$ by using a interpolation procedure;
(3) computing $\hat{\mathbf{y}}_{d,j} = \mathbf{D}_j\, \hat{\mathbf{y}}_{t,j}$ for the levels $j = 1, 2, ..., l$;
(4) adding the vectors $\hat{\mathbf{y}}_{d,j}$ for the levels $j = 1, 2, ..., l-1$ to their son level by using a filter procedure. Finally the vector $\hat{\mathbf{y}}_{d,l}$ contains the contributions of all levels;
(5) computing the vector $\hat{\mathbf{y}} = \mathbf{N}_l\, \hat{\mathbf{x}} + \mathbf{S}_l\, \hat{\mathbf{y}}_{d,l}$.

In the following we explain the interpolation and filter procedures used in steps 2 and 4. On a given level, say the level j, the vector $\hat{\mathbf{y}}_{t,j}$ or $\hat{\mathbf{y}}_{d,j}$ consists of M_j sub vectors with M_j being the number of clusters on the level j. Each sub vector contains m_j components with m_j being the number of integration points on the unit sphere surface $\mathbb{S}$. The number of integration points on the unit sphere surface $\mathbb{S}$ for each level is given by $m_j = 2\, N_j^2$ with N_j denoting the number of terms included in the equation (18) for the level j. As a father level contains fewer clusters but requires more integration points on the unit sphere surface $\mathbb{S}$ than its son level and the clusters of the father level have different center points to their sons, the interpolation procedure, by which the vector $\hat{\mathbf{y}}_{t,j}$ is computed from $\hat{\mathbf{y}}_{t,j+1}$, consists of two steps:

(1) interpolating each sub vector of the vector $\hat{\mathbf{y}}_{t,j+1}$ on the son level from its m_{j+1} components to m_j components;
(2) changing the reference center for the interpolated sub vector from the center of the cluster corresponding to it on the level $j+1$ to the center of the father cluster by using (16), adding the result to the sub vector corresponding to the father cluster.

The filter procedure, by means of which the vector $\hat{\mathbf{y}}_{d,j}$ for a son level is computed from $\hat{\mathbf{y}}_{d,j-1}$ of its father level, consists also of two steps:

(1) changing the reference center for each sub vector of the vector $\hat{\mathbf{y}}_{d,j-1}$ from the center of the corresponding cluster to the center of one of its son clusters by using (16);
(2) filtering the in the first step transformed sub vector $\hat{\mathbf{y}}_{d,j-1}$ from its m_{j-1} components to m_j components and adding the result to the sub vector corresponding to the son cluster.

These two steps must be applied to all son clusters of each cluster on the level $j-1$.

The interpolation and filtering can be realized numerically by using the spherical harmonic functions[31 13], defined as

$$Y_n^m(\phi,\theta) = \frac{1}{\sqrt{2\pi}}\bar{P}_n^m(sin\theta)e^{im\phi}, \tag{27}$$

where $\bar{P}_n^m$ denotes the normalized Legendre function[28],

$$\bar{P}_n^m(x) = (-1)^m\sqrt{(n+\frac{1}{2})\frac{(n-m)!}{(n+m)!}}p_n^m(x) \tag{28}$$

with $p_n^m(x)$ the Legendre function of degree n and order m. The functions $Y_n^m(\phi,\theta)$ form a orthonormal basis for square integrable functions on the surface of the unit sphere $\mathbb{S}$, so any such function can be developed to

$$f(\phi,\theta) = \sum_{n=0}^{\bar{N}-1}\sum_{m=-n}^{n} f_n^m Y_n^m(\phi,\theta), \tag{29}$$

with a properly chosen $\bar{N}$. Supposing that values of $f(\phi,\theta)$ are given at a latitude-longitude grid of $I*J$ points, i.e. $f(\phi_i,\theta_j)$ for $i=0,1,...,I-1$ and $j=0,1,...,J-1$ are known, f_n^m can be computed by using the FFT in the ϕ-direction and the Gauss-Legendre integration in the θ-direction:

$$f_n^m = \int_{\mathbb{S}} Y_n^{*m} f ds \approx \sqrt{2\pi}\sum_{j=0}^{J-1}\bar{P}_n^{*m}(x_j)w_j[\frac{1}{I}\sum_{k=0}^{I-1} f(x_j,\phi_k)e^{-i2\pi mk}], \tag{30}$$

where $*$ denotes the complex conjugate, $x_j = \sin(\theta)$ and w_j is the Gauss-Legendre weight for the integration point x_j. The values in the square brackets on the right hand side of (30) can be evaluated by using FFT. Now the values of the function f at another latitude-longitude grid of $\bar{I}*\bar{J}$ points can be computed as

$$f(\phi_{\bar{i}},\theta_{\bar{j}}) = \sum_{n=0}^{\bar{N}-1}\sum_{m=-n}^{n} f_n^m Y_n^m(\phi_{\bar{i}},\theta_{\bar{j}}) = \sum_{m=-(\bar{N}-1)}^{\bar{N}-1}\sum_{n=|m|}^{\bar{N}-1} f_n^m Y_n^m(\phi_{\bar{i}},\theta_{\bar{j}}). \tag{31}$$

Inserting (27) in the right hand side of (31) gives

$$f(\phi_{\bar{i}},\theta_{\bar{j}}) = \sum_{m=-(\bar{N}-1)}^{\bar{N}-1}[\sum_{n=|m|}^{\bar{N}-1}\frac{1}{\sqrt{2\pi}} f_n^m \bar{P}_n^m(\sin\theta_{\bar{j}})]e^{im\phi_{\bar{i}}}. \tag{32}$$

Having computed f_n^m by using (30), the summation in the square brackets on the right hand side of (32) can be easily evaluated. Denoting this summation by $f^m(\theta_{\bar{j}})$ and inserting $\phi_{\bar{i}} = 2\pi\bar{i}/\bar{I}$ $(\bar{i} = 0, 1, ..., \bar{I} - 1)$ in (32) give

$$f(\phi_{\bar{i}}, \theta_{\bar{j}}) = \sum_{m=-(\bar{N}-1)}^{\bar{N}-1} f^m(\theta_{\bar{j}}) e^{i2\pi m\bar{i}/\bar{I}}, \ (\bar{i} = 0, 1, ..., \bar{I} - 1). \tag{33}$$

If $\bar{N} \leq \bar{I}$, (33) can be computed by using the inverse FFT (for the summation from 0 to $\bar{N} - 1$) and the FFT (for the summation from $-(\bar{N} - 1)$ to -1). Our numerical experiments indicate that $\bar{N} = N$ is a good choice for the value of $\bar{N}$ with N the number of terms in (18) for the son level in the above mentioned interpolation and the filtering procedures. So the condition $\bar{N} \leq \bar{I}$ is practically always fulfilled. For computing the Legendre function $p_n^m(x)$ in (28) the recurrence relation 8.5.3 in[28]

$$(n - m + 1)P_{n+1}^m(x) = (2n + 1)xP_n^m(x) - (n + m)P_{n-1}^m(x) \tag{34}$$

can be used and is proved to be stable whereas recurrence relation 8.5.1 in[28]

$$P_n^{m+1}(x) = [(n - m)xP_n^m(x) - (n + m)P_{n-1}^m(x)]/\sqrt{x^2 - 1} \tag{35}$$

is unstable for x in the vicinity of 1.

The above interpolation/filter procedure using the spherical harmonic functions is stable and precise but computationally quite expensive. Instead we have investigated the possibility of storing all the matrices $\mathbf{T}_j$, $\mathbf{D}_j$ and $\mathbf{S}_j$ on each level, in order to avoid the interpolation/filter procedures. This new scheme of the MLFMBEM is called by us as the direct MLFMBEM (DMLFMBEM), whereas the scheme with interpolation/filter procedures as indirect MLFMBEM (IMLFMBEM). Numerical tests indicate that the DMLFMBEM is substantially faster than the IMLFMBEM, whereas the storage requirements can be kept in the reasonable range. Because, for a given mesh and a given frequency, the nonzero elements of the matrices $\mathbf{T}_j$ and $\mathbf{S}_j$ increase with the size of the clusters (approximately) linearly, finer clusters on each level are preferable, when the DMLFMBEM is used.

5. Numerical Examples

In this section we show the results obtained for two examples. The first example is applied to compute the acoustic radiation from a horn (see Fig. 3).

The horn consists of a chamber (a closed cylinder, modeled with surface elements) and the 'horn body' (a shell with irregular section, modeled with middle face elements). The bottom of the chamber (a circle plate) vibrates with a constant normal velocity of 0.00871 mm/s. The chamber has a height of 40 mm and a diameter of 30mm. The horn body has a height of 306 mm and a bottom dimension of 148 $mm \times 154$ mm. The surfaces of all parts are assumed to be acoustically hard (admittance is zero). As there are two symmetry planes, only a quarter of the structure needs to be modeled. The boundary element mesh contains 2053 triangle constant elements (1973 middle face elements for the horn body

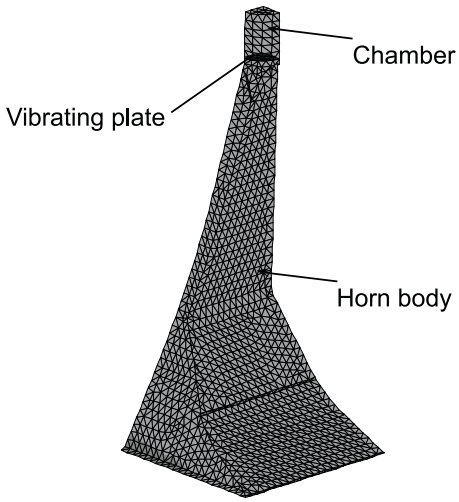

Fig. 3. Horn - quarter model

and 80 surface elements for the surface of the closed cylinder). The CGS-solver with ILU-preconditioning is used for solving the equation system. Sound radiation from the horn is computed in the frequency domain of 500 Hz to 10196 Hz with 88 steps. In Fig. 4 the sound powers obtained by using the traditional BEM, SLFMBEM, IMLFMBEM (2 levels) and DMLFMBEM (2 levels) are compared (the curves B and C are moved respectively 4 dB and 8 dB downwards). We notice, that the results of the 4 approaches coincide very well except for some low frequencies. At very low frequencies the FMBEM (especially the MLFMBEM) algorithm becomes less stable because of the singularity of the spherical Hankel function $h_j(k\|\mathbf{z}_2 - \mathbf{z}_1\|)$ appearing in (18) at the zero point.

Table 1 contains the run time statistic for the job with the 88 frequencies computed on a Dual Opteron machine with Debian Linux 64 and the nonzero entries of the coefficient matrices at the highest frequency (10196 Hz). For this small job (with 2053 unknowns) the SLFMBEM, IMLFMBEM and DMLFMBEM achieve an acceleration factor of 7.6, 4.3 and 8.2 times respectively. Although the SLFMBEM, IMLFMBEM and especially the DMLFMBEM need more storage space than the traditional BEM, it is not a serious problem, because storage requirements of the FMBEM schemes (especially of the IMLFMBEM and DMLFMBEM) increase only moderately with the number of unknowns (see the table 2 for a job with 47242 unknowns).

The second example shows the application of the FMBEM to compute the so called head-related transfer function[32]. At the first stage of the investigation we use an artificial head (see Fig. 5) instead of a real head for the simulation. Incident waves from 88 different directions are considered.

We define the HRTF as the ratio of the real sound pressure at the middle point of the entrance of an ear channel to the sound pressure at a reference point due to the incident

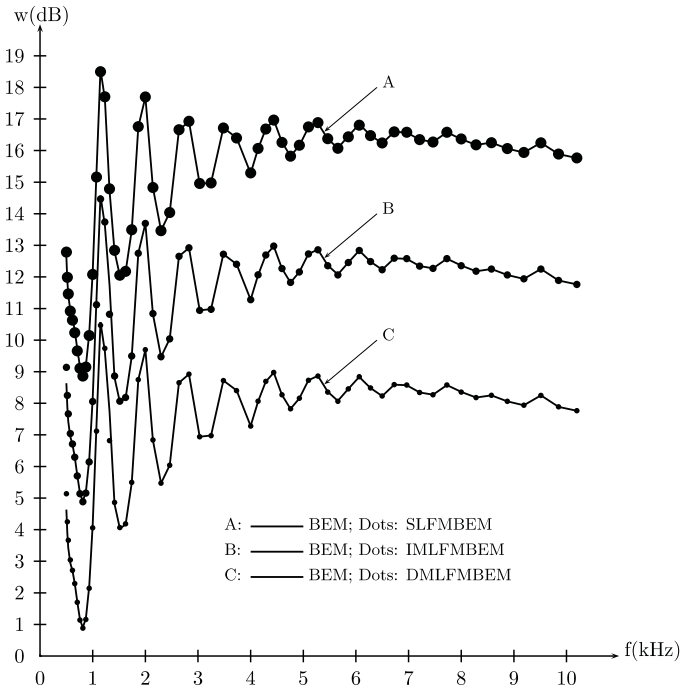

Fig. 4. Horn - Sound power of the horn

Table 1. Run time and number of nonzero entries of the coefficient matrices at 10196 Hz for the example horn.

	generating the equation system (s)	solving the equation system (s)	post processing (s)	whole job (s)	nonzero entries (10^6)
BEM	7415	392	7142	14949	4.21
SLFMBEM	563	577	819	1961	7.00
IMLFMBEM	340	2587	577	3505	4.56
DMLFMBEM	343	837	643	1824	10.52

wave only. The reference point is chosen as the middle point of the line connecting the middle points of the entrances of the two ear channels. Admittance of the surface of the head model is assumed to be zero. It is discretized with a mesh consisting of 47242 4-sided surface elements, so that sound reflection from the head can be computed up to 20,000 Hz with sufficient accuracy (more than 6 elements per wave length). The incident waves from different directions are simulated by using point monopole sound sources situated in a sphere surface with the above mentioned reference point as center and a radius of 1.2 m (all together 88 such sound sources). In order to treat all the incident directions in one

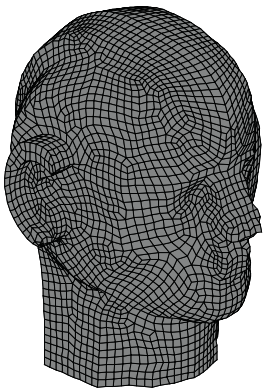

Fig. 5. The artificial head

computation run, the following reciprocity relation is derived

$$p_{oq} = \frac{-qp_{qo}}{i\omega\rho A_o v_{no}}, \tag{36}$$

where q is the intensity of the sound source, A_o is the area of the only element which vibrates (with the normal velocity v_{no}). p_{qo} and p_{oq} represent the sound pressure at the point source due to the vibrating element and the sound pressure at the center of the vibrating element due to the point source respectively. By means of (36), the computation of the sound pressures at the entrance of the ear channel due to different point sources is converted to computation of the sound pressures at the sound sources due to the vibrating element that is located at the entrance of the ear channel. The method of computing the sound pressures at the entrance of the ear channel due to different point sources indirectly by means of the reciprocity relation (36) is referred to in the following as the indirect method. As the reciprocity relation is analytic, the accuracy of the numerical computations can be examined by comparing the results of the direct and indirect methods: when the numerical results are accurate within a given tolerance, the results of the direct and the indirect methods must coincide within about the same tolerance. Fig. 6 shows the sound pressures at the entrance of the right ear channel obtained by using the direct and indirect methods for 4 directions in the horizontal plane (computed by using the DMLFMBEM with 3 levels). It can be seen that the agreement between the two methods is good except for the direction 'left' at the frequencies above 8000 Hz, where the sound pressure is too small to be computed accurately.

In Fig. 7 the HRTFs for 4 directions in the median plane obtained by using the SLFMBEM and DMLFMBEM (with 3 levels) are compared. The agreement between the two methods is very good in the whole frequency domain for all four directions.

The run time for computing the HRTFs at 36 frequencies between 500 Hz and 18000 Hz on a Dual Opteron machine with Debian Linux 64 as well as the number of the nonzero

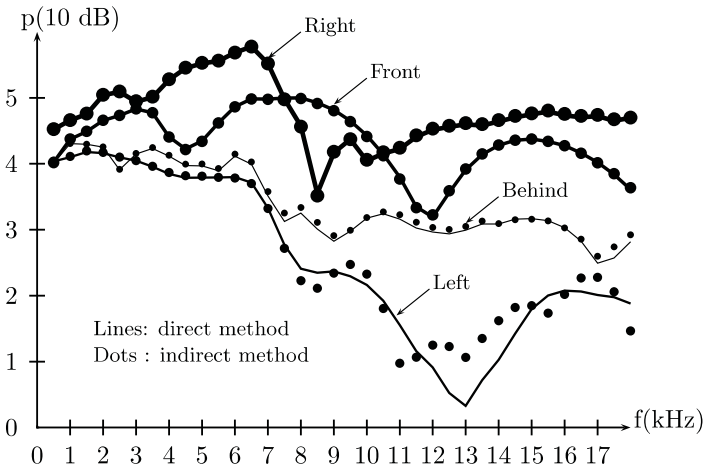

Fig. 6. Comparison of the results of the direct and indirect methods

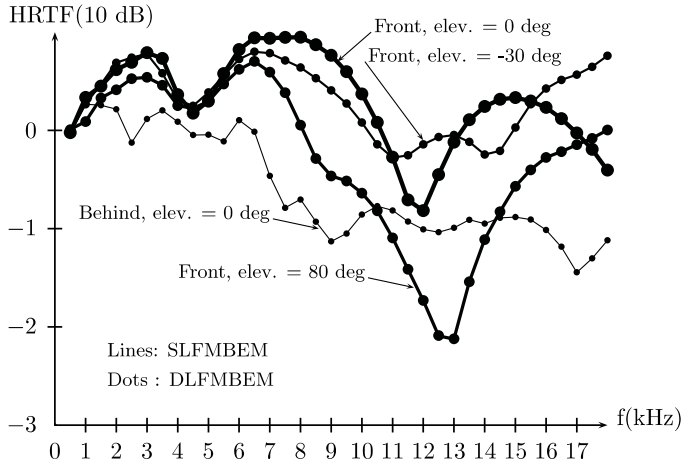

Fig. 7. HRTF for 4 directions in the median plane

components of the coefficient matrices at the last frequency (18000 Hz) are listed in table 2. The IMLFMBEM is superior to the SLFMBEM for this example (with 47247 unknowns) in terms of CPU-times and storage requirements. The DMLFMBEM achieves an acceleration factor of 2.6 and 1.9 over the SLFMBEM and the IMLFMBEM respectively, whereas its storage requirements is only slightly higher than that of the SLFMBEM.

Table 2. Run time and number of nonzero entries of the coefficient matrices at 18000 Hz for the example HRTF.

	generating the equation system (s)	solving the equation system (s)	post processing (s)	whole job (s)	nonzero entries (10^6)
SLFMBEM	25493	9861	910	36283	235.36
IMLFMBEM	5499	19211	910	25638	86.67
DMLFMBEM	4223	7765	1732	13739	258.43

6. Conclusion

The SLFMBEM and MLFMBEM are successfully applied to a Burton-Miller formulation of the collocation BEM for acoustic problems in the frequency domain, by which both the surfaces of 3-dimensional domains and the middle faces of thin walled parts are considered. The application of the FMBEM can drastically reduce the number of operations and the storage requirements for large scale problems while the accuracy of the results is not deteriorated except at very low frequencies. At very low frequencies the FMBEM algorithm becomes less accurate because of the singularity of the spherical Hankel functions at zero. Behaviors of three schemes of the FMBEM (SLFMBEM, IMFMBEM and DMLFMBEM) are compared by means of two examples. We notice that all the schemes provide reliable results, however the DMLFMBEM, where the coefficient matrices at each level are stored and therefore the interpolation and filtering procedures between the father and son levels are avoided, is substantially faster than the other two schemes, whereas is storage requirements can be controlled within the reasonable domain.

7. Acknowledgment

This study was funded by the Austrian Academy of Sciences and partly by the Austrian Science Fund, FWF, project number P18401-B15.

References

1. V. Rokhlin, Rapid Solution of Integral Equations of classical potential theory, *Comput. Phys.* **60** (1983) 187.
2. V. Rokhlin, Rapid Solution of Integral Equations of Scattering Theory in Two Dimensions, *J. Comput. Phys.* **86** (1990) 414.
3. V. Rokhlin, Diagonal Forms of Translation Operators for the Helmholtz Equation in Three Dimensions, *Appl. Comput. Harmonic Anal.* **1** (1993) 82.
4. R. Coifman, V. Rokhlin and S. A. Wandzura, The Fast Multipole Method for the Wave Equation: a Pedestrian Prescription, *IEEE Antennas Propag. Magaz.* **35**(3)(1993) 7.
5. M. A. Epton and B. Dembart, Multipole Translation Theory for the Three-Dimensional Laplace and Helmholtz Equations, *SIAM J. Sci. Comput.* **16**(4)(1995) 865.
6. J. Rahola, Diagonal Forms of the Translation Operators in the Fast Multipole Algorithm for Scattering Problems, *BIT* **36**(2) (1996) 333.
7. K. Giebermann, Schnelle Summationsverfahren zur numerischen Lösung von Integralgleichungen für Streuprobleme im $\mathbb{R}^3$, PhD. thesis, University Karlsruhe (1997).

8. J. Song, C.-C. Lu and W. C. Chew, Multilevel Fast Multipole Algorithm for Electromagnetic Scattering by Large Complex Objects, *IEEE Trans. Antennas Propagat.* **45**(10) (1997) 1488.
9. W. C. Chew, J.-M. Jin, C.-C. Lu, E. Michielssen, and J.M. Song, Fast Solution Method in Electromagnetics *IEEE Trans. Antennas Propagat.* **45**(3) (1997) 533.
10. L. Greengard, J. Huang, V. Rokhlin, and S. Wandzura, Accelerating Fast Multipole Methods for the Helmholtz Equation at Low Frequencies, *IEEE Comput. Sci. Engng.* **5**(3) (1998) 32.
11. S. Koc and W. C. Chew, Calculation of Acoustic Scattering from a Cluster of Scatterers, *J. Acoust. Soc. Am.* **103**(2) (1998) 721.
12. M. F. Gyure and M. A. Stalzer, A Prescription for the Multilevel Helmholtz FMM, *IEEE Comput. Sci. Engng.* **5**(3)(1998) 39.
13. E. Darve, The Fast Multipole Method I: Error analysis and Asymptotic Complexity, *SIAM J. Numer. Anal.* **38**(1) (2000) 98.
14. T. Sakuma and Y. Yasuda, Fast Multipole Boundary Element Method for Large-Scale Steady-State Sound Field Analysis. Part I: Setup and Validation, *Acta Acustica united with Acustica* **88** (2002) 513.
15. Y. Yasuda and T. Sakuma, Fast Multipole Boundary Element Method for Large-Scale Steady-State Sound Field Analysis. Part1 II: Examination of Numerical Items, *Acta Acustica united with Acustica* **89** (2003) 28.
16. S. Schneider, Application of Fast Method for Acoustic Scattering and Radiation Problems, *J. Comput. Acoust.* **11**(3) (2003) 387.
17. M. Fischer, U. Gauger and L. Gaul, A Multipole Galerkin Boundary Element Method for Acoustics, *Engineering Analysis with Boundary Elements* **28** (2004) 155.
18. Y. Yasuda and T. Sakuma, An Effective Setting of Hierarchical Cell Structure for the Fast Multipole Boundary Element Method, *J. Comput. Acoust.* **13**(1) (2005) 47.
19. M. Fischer and L. Gaul, Application of the Fast Multipole BEM for Structural-Acoustic Simulations, *J. Comput. Acoust.* **13**(1)(2005) 87.
20. A. J. Burton and G. F. Miller, The application of integral equation methods to the numerical solution of some exterior boundary-value problems, *Proc. Roy. Soc. Lond.* **A 323** (1971) 201.
21. H. A. Schenck, Improved integral formulation for acoustic radiation problem, *J. Acoust. Soc. Am.* **44**(1) (1968) 41.
22. S. Marburg and S. Schneider, Influence of Element Types on Numeric Error for Acoustic Boundary Elements, *J. Comput. Acoust.* **11**(3) (2003) 363.
23. Z.-S. Chen and H. Waubke, A Burton-Miller Collocation Formulation of FMM for the Acoustic Problems, in *Computational Mechanics (CD-Rom)*, eds. Z. H. Yao, M. W. Yuan and W. X. Zhong (Tsinghua University Press, Beijing, 2004), MCCMVI_CDROM_1(E:)/MS_PDF/M-216.
24. Y. Yasuda and T. Sakuma, A Technique for Plane-Symmetric Sound Field Analysis in the Fast Multipole Boundary Element Method, *J. Comput. Acoust.* **13**(1) (2005) 71.
25. Z.-S. Chen, G. Hofstetter and H. A. Mang, A symmetric Galerkin Formulation of the boundary element method for acoustic radiation and scattering, *J. Comput. Acoust.* **5**(2) (1997) 219.
26. G. Krishnasamy, L.W. Schmerr, T. J. Rudolphi, and F. J. Rizzo, Hypersingular Boundary Integral Equations: Some Applications in Acoustic and Elastic Wave Scattering, *J. Appl. Mech.* **57** (1990) 404.
27. A. Meister, *Numerik linearer Gleichungssysteme* (Friedr. Vieweg & Sohn Verlagsgesellschaft GmbH, Braunschweig/Wiesbaden, 1999).
28. M. Abramowitz and I. A. Stegun, *Handbook of Mathematical Functions* Dover Publications, INC., New Yourk, 1972.
29. S. Marburg and S. Schneider, Performance of iterative solvers for acoustic problems. Part I. Solvers and effect of diagonal preconditioning, *Engineering Analysis with Boundary Elements* **27** (2003) 727.

30. S. Schneider and S. Marburg, Performance of iterative solvers for acoustic problems. Part II. Acceleration by ILU-type preconditioner *Engineering Analysis with Boundary Elements* **27** (2003) 751.
31. R. Jacob-Chien and B. K. Alpert, A Fast Spherical Filter with Uniform Resolution, *J. Comput. Phys.* **136** (1997) 580.
32. B. F. G. Katz, Boundary Element Method Calculation of Individual Head-Related Transfer Function. I. Rigid Model Calculation, *J. Acoust. Soc. Am.* **110**(5) (2001) 2440.